The Journal of Chemical Physics

Reduced density-matrix functional theory: Correlation and spectroscopy

Cite as: J. Chem. Phys. **143**, 024108 (2015); https://doi.org/10.1063/1.4926327
Submitted: 21 March 2015 • Accepted: 24 June 2015 • Published Online: 13 July 2015

S. Di Sabatino, J. A. Berger, L. Reining, et al.


View Online

Export Citation

CrossMark

ARTICLES YOU MAY BE INTERESTED IN

Benchmark calculations for reduced density-matrix functional theory
The Journal of Chemical Physics **128**, 184103 (2008); https://doi.org/10.1063/1.2899328

A universal density matrix functional from molecular orbital-based machine learning: Transferability across organic molecules
The Journal of Chemical Physics **150**, 131103 (2019); https://doi.org/10.1063/1.5088393

The density matrix renormalization group in chemistry and molecular physics: Recent developments and new challenges
The Journal of Chemical Physics **152**, 040903 (2020); https://doi.org/10.1063/1.5129672

AIP Publishing

© 2015 AIP Publishing LLC.

Reduced density-matrix functional theory: Correlation and spectroscopy

S. Di Sabatino,[1] J. A. Berger,[2] L. Reining,[3] and P. Romaniello[1]
[1]*Laboratoire de Physique Théorique, CNRS, IRSAMC, Université Toulouse III–Paul Sabatier, 118 Route de Narbonne, 31062 Toulouse Cedex, France and ETSF*
[2]*Laboratoire de Chimie et Physique Quantiques, IRSAMC, Université Toulouse III–Paul Sabatier, CNRS, 118 Route de Narbonne, 31062 Toulouse Cedex, France and ETSF*
[3]*Laboratoire des Solides Irradiés, École Polytechnique, CNRS, CEA-DSM, 91128 Palaiseau, France and ETSF*

(Received 21 March 2015; accepted 24 June 2015; published online 13 July 2015)

In this work, we explore the performance of approximations to electron correlation in reduced density-matrix functional theory (RDMFT) and of approximations to the observables calculated within this theory. Our analysis focuses on the calculation of total energies, occupation numbers, removal/addition energies, and spectral functions. We use the exactly solvable Hubbard dimer at 1/4 and 1/2 fillings as test systems. This allows us to analyze the underlying physics and to elucidate the origin of the observed trends. For comparison, we also report the results of the *GW* approximation, where the self-energy functional is approximated, but no further hypothesis is made concerning the approximations of the observables. In particular, we focus on the atomic limit, where the two sites of the dimer are pulled apart and electrons localize on either site with equal probability, unless a small perturbation is present: this is the regime of strong electron correlation. In this limit, using the Hubbard dimer at 1/2 filling with or without a spin-symmetry-broken ground state allows us to explore how degeneracies and spin-symmetry breaking are treated in RDMFT. We find that, within the used approximations, neither in RDMFT nor in *GW*, the signature of strong correlation is present, when looking at the removal/addition energies and spectral function from the spin-singlet ground state, whereas both give the exact result for the spin-symmetry broken case. Moreover, we show how the spectroscopic properties change from one spin structure to the other. © *2015 AIP Publishing LLC.* [http://dx.doi.org/10.1063/1.4926327]

I. INTRODUCTION

Strongly correlated electron systems exhibit remarkable electronic and magnetic properties, such as metal-insulator transitions, half-metallicity, or unconventional superconductivity, which make them among the most attractive and versatile materials (see, e.g., Refs. 1–3). Typically, these materials have incompletely filled d- or f-electron shells with narrow energy bands. In this case, a theoretical description based on current mean-field or perturbation approaches is not enough and a more accurate treatment of electron correlation is required.[4–7] This represents one of the greatest challenges in condensed-matter physics today.

One of the most popular approaches in this field is many-body perturbation theory (MBPT) based on Green's functions. Within the so-called *GW* approximation[8] to electron correlation, MBPT has become, over the last two decades, the tool of choice for the calculations of quasiparticle (QP) band structures[9–14] and direct and inverse photo-emission spectra[4,15–18] of many materials improving substantially over the results provided by static mean-field electronic structure methods. However, *GW* suffers from some fundamental shortcomings,[19–24] and, in particular, it is not expected to describe strong correlation. More refined levels of approximations are hence needed and much effort is devoted to this goal both by going beyond standard methods[5,25–30] and by exploring novel routes to calculate Green's functions.[31,32] In this context, promising results for solids have been reported using reduced density-matrix functional theory (RDMFT).[33]

Within RDMFT, the ground-state properties of a physical system are functionals of the ground-state one-body density matrix,[34,35] since there exists a one-to-one mapping between the (non-degenerate) ground-state wavefunction of the system and the corresponding density matrix.[35] In particular, the ground-state total energy is a functional of the one-body density matrix γ and it can be written as $E[\gamma] = E_{\text{kin}}[\gamma] + E_{\text{ext}}[\gamma] + E_{\text{H}}[\gamma] + E_{\text{xc}}[\gamma]$, where E_{kin}, E_{ext}, E_{H}, and E_{xc} are the kinetic energy, the energy due to the coupling to an external potential, and the Hartree and exchange-correlation energies, respectively. Energy minimization under the constraint that γ is N-representable determines the exact γ. In practice, however, approximations to $E_{\text{xc}}[\gamma]$ are needed. Several approximations have been proposed and most of them are implicit functionals of the density matrix; they are explicit functionals of the natural orbitals[34] ϕ_i and occupation numbers n_i, i.e., the eigenfunctions and eigenvalues, respectively, of the density matrix, $\gamma(\mathbf{x},\mathbf{x}') = \sum_i n_i \phi_i(\mathbf{x})\phi_i^*(\mathbf{x}')$. The total energy is then a functional of ϕ_i and n_i. Once the density matrix of the system is known, all the observables of the system can be calculated, provided that their expression as functional of the density matrix is known.

Such a functional has not been found yet for the spectral function, which determines, for example, photoemission spectra. Various ways to calculate removal/addition energies

 © 2015 AIP Publishing LLC

have been proposed.[33,36] For example, removal energies can be calculated by using the method proposed by Pernal and Cioslowski,[36] which is based on the extended Koopmans theorem (EKT).[37,38] So far, the method has been used only for finite systems. Numerical evidence suggests that EKT is at least exact for the lowest ionization potential.[39–42] In Ref. 33, an approximate procedure to calculate quasiparticle energies and photoemission spectra within RDMFT has been proposed, which is also inspired by Koopmans theorem. When applied to a series of transition-metal oxides, the method seems to capture the essential physics of strong electron correlations. These are, however, only empirical evidences, and an in-depth analysis is missing. This is not simple because several approximations are involved: (i) an approximate exchange-correlation energy functional, (ii) an approximate expression for the removal and addition energies, and (iii) an approximate expression for the spectral function. It is therefore important to study these aspects in a systematic way in order to advance our understanding of an approach which is used all over physics and chemistry.

To do this, we need a simpler system, preferably with a known exact solution for benchmarking, with a direct link between the molecular orbitals and natural orbitals and with the possibility to study quasi-degeneracies and (spin and charge) symmetry breaking. An ideal candidate is the Hubbard dimer: it is exactly solvable, the natural orbitals correspond to the bonding/antibonding orbitals, and the atomic limit $t \to 0$ offers a playground to explore degeneracies and symmetry breaking. In the atomic limit, when the two sites are pulled apart, electrons localize on either site with equal probability, unless a small perturbation is present. In this limit, explicit correlation between particles is crucial: this is the regime of strong electron correlation. In this limit, all the eigenstates of the system at 1/4 filling acquire equal energy and they become degenerate with the charge-symmetry broken states; at 1/2 filling, the spin-singlet ground state becomes degenerate with the spin-triplet state as well as with the spin-symmetry-broken states (see Tables I and II in Ref. 20). This scenario is general and common also to other molecules, such as, e.g., H_2 at dissociation, which is a paradigmatic example in quantum chemistry (see, e.g., Refs. 22 and 43–51). Analogies can be found also in infinite systems, as, for example, in the homogeneous electron gas (HEG). In the HEG, the analogous of the bonding/antibonding orbitals are the eigenstates of the perfectly translationally invariant system, which are also the natural orbitals. At low densities, electrons localize to minimize the electron-electron interaction and the translational symmetry is spontaneously broken.

In the following, therefore, we will use the Hubbard dimer at 1/4 and 1/2 fillings as a test case, and we will suggest extrapolation to real systems when appropriate.

The paper is organized as follows. In Sec. II, we will report the key equations of MBPT and RDMFT. In Sec. III, MBPT and RDMFT results for occupation numbers, total energy, removal/addition energies, and spectral function are compared to exact results and analyzed. In Sec. IV, we discuss how correlation is related to the measurements a physical system is subjected to. Finally, we extrapolate these considerations to real systems. Conclusions are given in Sec. V.

II. THEORETICAL FRAMEWORK

In the following, we will give the key equations used in many-body perturbation theory and reduced density-matrix functional theory, and, in particular, we will discuss how one can calculate ground- and excited-state properties, namely, total energy, occupation numbers, removal and addition energies, and spectral function in the two approaches. We will use atomic units $\hbar = m = e = 1$ and work at zero temperature throughout the paper.

A. MBPT

Within MBPT, the leading role is played by the one-body Green's function G. At zero temperature, the time-ordered equilibrium Green's function [52] reads as

$$G(1,2) \equiv -i \langle \Psi_0 | \mathcal{T}[\hat{\psi}(1)\hat{\psi}^\dagger(2)] | \Psi_0 \rangle , \tag{1}$$

where $\mathcal{T}$ is the time-ordering operator, Ψ_0 is the ground-state many-body wavefunction, $\hat{\psi}$ and $\hat{\psi}^\dagger$ are field operators in the Heisenberg picture. Here, $(1) \equiv (\mathbf{x}_1, t_1) \equiv (\mathbf{r}_1, s_1, t_1)$ and $(1^+) \equiv (\mathbf{x}_1, t_1^+)$ with $t_1^+ \equiv t_1 + \delta$ $(\delta \to 0^+)$ describe space, spin, and time coordinates. G contains a wealth of information about a physical system. In particular, the ground-state total energy E_0 can be obtained using the Galitskii-Migdal formula

$$E_0 = -\frac{i}{2} \int d\mathbf{x}_1 \lim_{2 \to 1^+} \left(i \frac{\partial}{\partial t_1} + h_0(\mathbf{r}_1) \right) G(1,2), \tag{2}$$

where $h_0(\mathbf{r}_1) = -\nabla_{\mathbf{r}_1}/2 + v_{\text{ext}}(\mathbf{r}_1)$ is the one-body Hamiltonian. Moreover, we are also interested in the density matrix $\gamma(\mathbf{x}_1, \mathbf{x}_2) = -iG(1, \mathbf{x}_2 t_1^+) = -i \int d\omega/(2\pi)\, G(\omega) e^{i\omega 0^+}$ and the spectral function $A(\omega) = |\Im G(\omega)|/\pi$, which is closely related to photoemission spectra.[53]

Equation (1) is not practical to determine G, since it requires the knowledge of the many-body wavefunction. In MBPT, one uses instead the Dyson equation $G = G_0 + G_0 \Sigma G$, where G_0 is the non-interacting one-body Green's function and Σ is the self-energy, which describes all the many-body effects of the system. Approximations to the self-energy are needed, and a very popular one is $\Sigma = v_{\text{H}} + iGW$, where v_{H} is the Hartree potential and $W = \epsilon^{-1} v_c$ is the dynamically screened Coulomb interaction, with ϵ^{-1} the inverse dielectric function and v_c the bare Coulomb interaction.[8] In Sec. III, we will compare the exact results obtained using (1) with those obtained from the GW approximation. The GW equations should, in principle, be solved self-consistently, since the self-energy is a functional of the one-body Green's function. Here, we solve the GW equations without self-consistency, using G_0 to build W and Σ: $\Sigma = v_{\text{H}} + iG_0W_0$, with $v_{\text{H}} = -iv_cG_0$ and $W_0 = [1 + iv_cG_0G_0]^{-1} v_c$. This approach is called G_0W_0 or one-shot GW, and it is often used in practice.[75]

B. RDMFT

The reduced p-body density matrix is defined as

$$\Gamma^{(p)}(\mathbf{x}_1, \ldots, \mathbf{x}_p, \mathbf{x}_1', \ldots, \mathbf{x}_p') \equiv \binom{N}{p} \int d\mathbf{x}_{p+1}, \ldots, d\mathbf{x}_N \Psi^*(\mathbf{x}_1', \ldots, \mathbf{x}_p', \mathbf{x}_{p+1}, \ldots, \mathbf{x}_N) \times \Psi(\mathbf{x}_1, \ldots, \mathbf{x}_p, \mathbf{x}_{p+1}, \ldots, \mathbf{x}_N).$$

Within RDMFT,[35] the ground-state total energy is a unique functional of the one-body density matrix $\gamma \equiv \Gamma^{(1)}$. It reads as

$$E[\gamma] = E_{\rm kin}[\gamma] + E_{\rm ext}[\gamma] + \int d\mathbf{x}\, d\mathbf{x}'\, v_c(\mathbf{x},\mathbf{x}')\Gamma^{(2)}[\gamma](\mathbf{x},\mathbf{x}';\mathbf{x},\mathbf{x}'),$$

with

$$\Gamma^{(2)}[\gamma](\mathbf{x},\mathbf{x}';\mathbf{x},\mathbf{x}') = \frac{1}{2}\gamma(\mathbf{x},\mathbf{x})\gamma(\mathbf{x}',\mathbf{x}') + \Gamma^{(2)}_{\rm xc}[\gamma](\mathbf{x},\mathbf{x}';\mathbf{x},\mathbf{x}'). \tag{3}$$

The first and second terms on the right-hand side of (3) are the Hartree and exchange-correlation contributions, respectively. The latter is not known and needs to be approximated. Various approximations have been proposed in the literature.[54–60] Many of them, however, can be traced back to the work of Müller[61,76] and are based on the factorization

$$\Gamma^{(2)}_{\rm xc}[\gamma](\mathbf{x},\mathbf{x}';\mathbf{x},\mathbf{x}') \approx -\frac{1}{2}\gamma^{\alpha}(\mathbf{x}',\mathbf{x})\gamma^{\alpha}(\mathbf{x},\mathbf{x}'), \tag{4}$$

where

$$\gamma^{\alpha}(\mathbf{x},\mathbf{x}') = \sum_j n_j^{\alpha}\phi_j(\mathbf{x})\phi_j^*(\mathbf{x}'),$$

where $\phi_i(\mathbf{x})$ and n_i are the naturals orbitals and the occupation numbers, respectively. Note that with $\alpha = 1$ in (4), one gets the Hartree-Fock approximation to $\Gamma^{(2)}$. The total energy can then be expressed as a functional of ϕ_i and n_i, $E[\{n_i\},\{\phi_i\}]$; functional minimization with respect to the natural orbitals, under orthonormality constraints, and occupation numbers, under total particle conservation and N-representability constraints ($0 \le n_i \le 1$), leads to the ground-state total energy E_0. In this work, we study approximation (4), with $0.5 \le \alpha \le 1$, which has been applied both to extended[33,58,60,62] as well as to finite systems (see, e.g., Refs. 36, 54, and 62–65). From the natural orbitals and occupation numbers which minimize the total energy, one can build the one-body density matrix that corresponds to a given approximation for $\Gamma^{(2)}$. The procedure to determine the one-body density matrix is then different from the standard one used for the Green's function, for which one solves a Dyson equation for a given approximation to the self-energy. Moreover, whereas one can extract information about photoemission spectra directly from the imaginary part of G, this is not the case in RDMFT. It does not yield G nor its imaginary part.

Natural occupation numbers are strictly related to the multideterminant nature of the wavefunction of a physical system. To illustrate this, let us expand the many-body wavefunction in terms of Slater determinants constructed from the eigenfunctions of the one-body density matrix $\{\phi_i\}$, $\Psi_0(\mathbf{x}_1,\ldots,\mathbf{x}_N) = \sum_i C_i\Phi_i(\mathbf{x}_1,\ldots,\mathbf{x}_N)$. The one-body density-matrix then reads[66] as

$$\begin{aligned}\gamma(\mathbf{x},\mathbf{x}') &= N\int d\mathbf{x}_2,\ldots,d\mathbf{x}_N \\ &\times \sum_{ij} C_i^*C_j\Phi_i^*(\mathbf{x}',\mathbf{x}_2,\ldots,\mathbf{x}_N)\Phi_j(\mathbf{x},\mathbf{x}_2,\ldots,\mathbf{x}_N) \\ &= \sum_i |C_i|^2\gamma_i(\mathbf{x},\mathbf{x}'),\end{aligned} \tag{5}$$

where $\gamma_i(\mathbf{x},\mathbf{x}') = \sum_k \phi_k^i(\mathbf{x})\phi_k^{i*}(\mathbf{x}')$ is the density matrix associated to the ith Slater determinant. If the wavefunction of the system is described by a single Slater determinant, as in the case of a single (spin-polarized) electron (see the Hubbard dimer at 1/4 filling in Sec. III A 1), then the natural occupation numbers are either 1 or 0. If instead more determinants are involved, the natural occupation numbers, in general, take fractional values between 0 and 1. This can be nicely illustrated by considering a two-electron system with a singlet wavefunction $\Psi_0(\mathbf{x}_1,\mathbf{x}_2) = \sum_{i=1,2} C_i\Phi_i(\mathbf{x}_1,\mathbf{x}_2)$, where $\Phi_1 = |b\uparrow, b\downarrow\rangle$ and $\Phi_2 = |a\uparrow, a\downarrow\rangle$ are Slater determinants constructed from bonding and antibonding orbitals $\{\phi_i\}$, respectively (see the Hubbard dimer at 1/2 filling in Sec. III A 2). Note that the bonding/antibonding orbitals in the Hubbard dimer correspond to the natural orbitals. The one-body density matrix reads as

$$\begin{aligned}\gamma(\mathbf{x},\mathbf{x}') &= |C_1|^2 \sum_{i=b\uparrow,b\downarrow} \phi_i(\mathbf{x})\phi_i^*(\mathbf{x}') + |C_2|^2 \sum_{i=a\uparrow,a\downarrow} \phi_i(\mathbf{x})\phi_i^*(\mathbf{x}') \\ &= \sum_{i=b\uparrow,b\downarrow,a\uparrow,a\downarrow} n_i\phi_i(\mathbf{x})\phi_i^*(\mathbf{x}'),\end{aligned} \tag{6}$$

with $n_{b\uparrow} = n_{b\downarrow} = |C_1|^2$ and $n_{a\uparrow} = n_{a\downarrow} = |C_2|^2$, and $|C_1|^2 + |C_2|^2 = 1$ since the wavefunction Ψ_0 is normalized. In general, the relation between C_i and natural occupation numbers is more complicated than in this example, but the fact that fractional occupation numbers reflect the multideterminant nature of the wavefunction and hence the degree of correlation in a system remains still valid.

Recently, Sharma *et al.*[33] proposed the following approximate expression for the spectral function within RDMFT:

$$A(\omega) \approx \sum_i \left[n_i\delta(\omega - \epsilon_i^-) + (1-n_i)\delta(\omega + \epsilon_i^+)\right], \tag{7}$$

where $\epsilon_i^{\pm} = E_0^N - E_i^{N\pm1}$, with E_0^N the ground-state energy of the N-electron system and $E_i^{N\pm1}$ the ith state energy of the $N \pm 1$-electron system. To arrive at Eq. (7), one starts from the exact expression $A(\omega) = |\Im G(\omega)|/\pi$ and approximates the ground and excited states of the $N+1$- and $N-1$-electron systems by adding an electron, $|\Psi_i^{N+1}\rangle = \frac{1}{\sqrt{1-n_i}}c_i^{\dagger}|\Psi_0^N\rangle$, or a hole, $|\Psi_i^{N-1}\rangle = \frac{1}{\sqrt{n_i}}c_i|\Psi_0^N\rangle$, to the ground state of the N-electron system. This is in the spirit of Koopmans theorem and it is an approximation, because, in general, the states obtained in this way are not eigenstates of the $N+1$- and $N-1$-electron system, respectively, and do not form a complete set. Along the same line, the energies ϵ_i^- and ϵ_i^+ in Eq. (7) are calculated in an approximate way as

$$\epsilon_k^- = -\epsilon_k^+ = \epsilon_k = E[\{n_i\},\{\phi_i\}]|_{n_k=1} - E[\{n_i\},\{\phi_i\}]|_{n_k=0}, \tag{8}$$

where $E[\{n_i\},\{\phi_i\}]|_{n_k=1}$ ($E[\{n_i\},\{\phi_i\}]|_{n_k=0}$) is the total energy for the N-particle system with all the occupation numbers fixed at their optimal value (i.e., the value that minimizes the energy functional) except for the occupation number n_k which is fixed to 1 (0). We will refer to this method as DIF (energy-DIFference), to keep contact with other works on the subject.[67] Using (8) for the calculation of removal and addition energies, the expression of the spectral function in (7) simplifies to $A(\omega) = \sum_i \delta(\omega - \epsilon_i)$.

We note that the energies calculated using Eq. (8) have both removal and addition characters, because, in general, the state k is partially filled. Equation (8) can, indeed, be rewritten as the sum of two contributions

$$\epsilon_k = \left(E[\{n_i\},\{\phi_i\}]|_{n_k=1} - E[\{n_i\},\{\phi_i\}]|_{n_k=n_k^{\text{opt}}} \right) + \left(E[\{n_i\},\{\phi_i\}]|_{n_k=n_k^{\text{opt}}} - E[\{n_i\},\{\phi_i\}]|_{n_k=0} \right), \quad (9)$$

where n_k^{opt} are the occupation numbers which minimize the total energy. The first term on the right-hand side of Eq. (9) corresponds to the addition of a fraction of electron equal to $1 - n_k^{\text{opt}}$ while the second to the removal of a fraction of electron equal to n_k^{opt}.

Moreover, the number of energies calculated using (8) equals the number of occupation numbers (i.e., the dimension of the natural orbital basis set), which is in general smaller than the exact number of removal and addition energies; it equals, indeed, the number of noninteracting states and hence the number of quasiparticles. Note that quasiparticle peaks in the spectral function can be directly linked to peaks in the non-interacting spectral function, whereas satellites are additional structures which are generated by the frequency-dependence of the self-energy and, therefore, have zero spectral weight for vanishing interaction. The spectral weight of a quasiparticle peak, instead, remains constant or might decrease by increasing the interaction, the weight being transferred to the satellites. This can be illustrated using the Hubbard dimer. As shown in Sec. III for this model system, the basis of natural orbitals $\{\phi_i\}$ diagonalizes also the one-body Green's function for any frequency; therefore, one can write

$$G(\mathbf{x}_1,\mathbf{x}_2;\omega) = \sum_i G_i(\omega)\phi_i(\mathbf{x}_1)\phi_i^*(\mathbf{x}_2), \quad (10)$$

and for the occupation numbers, one gets

$$n_i = -i \int \frac{d\omega}{2\pi} G_i(\omega) e^{i\omega 0^+}. \quad (11)$$

If G_i has more than one pole, then the total number of removal/addition energies that one should find is larger than the number of occupation numbers. Therefore, Equation (8), in general, describes a mixture of quasiparticle and satellite energies, as will be illustrated in Sec. III.

The total energy difference, Eq. (8), can be further approximated as

$$E[\{n_i\},\{\phi_i\}]|_{n_k=1} - E[\{n_i\},\{\phi_i\}]|_{n_k=0} \approx \left.\frac{\partial E}{\partial n_k}\right|_{n_k=1/2}, \quad (12)$$

which is justified if the total energy is linear in the occupation number n_k.[68] This method will be referred to as DER (energy DERivative). Using Eqs. (7) and (12), the spectral function of several transition metal oxides has been calculated, showing that some experimental features are captured.[33]

As an alternative to Eq. (8) (or (12)), removal energies can be calculated by using the EKT as proposed by Pernal and Cioslowski.[36] The method is based on the diagonalization of the Lagrangian matrix,

$$\Lambda_{ij} = \frac{1}{\sqrt{n_i n_j}} \left[n_i h_{0,ji} + 2 \sum_{klm} \Gamma^{(2)}_{iklm} v_{c,jkml} \right], \quad (13)$$

with $h_{0,ji} = \int d\mathbf{x}\, \phi_j^*(\mathbf{x}) h_0(\mathbf{x}) \phi_i(\mathbf{x})$,

$$\Gamma^{(2)}_{iklm} = \int d\mathbf{x}_1' d\mathbf{x}_2' d\mathbf{x}_1 d\mathbf{x}_2\, \Gamma^{(2)}(\mathbf{x}_1',\mathbf{x}_2';\mathbf{x}_1,\mathbf{x}_2) \times \phi_m^*(\mathbf{x}_2)\phi_l^*(\mathbf{x}_1)\phi_k(\mathbf{x}_2')\phi_i(\mathbf{x}_1'),$$

and

$$v_{c,jkml} = \int d\mathbf{x}_1 d\mathbf{x}_2 \phi_j^*(\mathbf{x}_1)\phi_k^*(\mathbf{x}_2) v_c(\mathbf{x}_1,\mathbf{x}_2)\phi_m(\mathbf{x}_1)\phi_l(\mathbf{x}_2).$$

The eigenvalues of Λ are the removal energies. The underlying physics of this method is similar to that of the approximations used to derive Eq. (7), although more advanced: in the EKT, the $N-1$-electron states are obtained as a linear combination of states obtained by removing an electron from the ground state of the N-electron system, $|\Psi^{N-1}\rangle = \sum_i B_i c_i |\Psi_0^N\rangle$; the energy of the so obtained $N-1$-electron states is minimized with respect to the coefficients B_i, unlike in the DIF/DER method. In practice, the EKT has only been applied to finite systems. For the Hubbard dimer at 1/4 and 1/2 fillings, it delivers the exact removal energies when combined with the exact exchange-correlation energy functional. Therefore, in this work, we will use it to test approximations to the xc energy functional. Note that the lowest addition energy can be obtained from the highest removal energy of the $N+1$-system (if the latter is stable).

III. CORRELATION IN THE HUBBARD DIMER

In this section, we will illustrate the physics behind different approximations to correlation as well as to observables in RDMFT and show how it compares with the standard G_0W_0 method used in MBPT. To this purpose, we use the Hubbard dimer, a simple prototype of a strongly correlated system that can be solved exactly.[69] The Hamiltonian of the Hubbard dimer reads as

$$H = -t \sum_{\substack{i,j=1,2 \\ i\neq j}} \sum_\sigma c_{i\sigma}^\dagger c_{j\sigma} + \frac{U}{2} \sum_{i=1,2} \sum_{\sigma,\sigma'} c_{i\sigma}^\dagger c_{i\sigma'}^\dagger c_{i\sigma'} c_{i\sigma} + \epsilon_0 \sum_{i=1,2} \sum_\sigma c_{i\sigma}^\dagger c_{i\sigma} + V_0. \quad (14)$$

Here, $c_{i\sigma}^\dagger$ and $c_{i\sigma}$ are the creation and annihilation operators for an electron at site i with spin σ, U is the on-site (spin-independent) interaction, $-t$ is the hopping kinetic energy, and ϵ_0 is the orbital energy. The Hamiltonian further contains a potential V_0 that can be chosen to fix the zero-energy scale. The physics of the Hubbard model[69] arises from the competition between the hopping term, which prefers to delocalize electrons, and the on-site interaction, which favours localization. The ratio U/t is a measure for the relative contribution of both terms and is the intrinsic, dimensionless coupling constant of the Hubbard model, which will be used in the following.

We refer to Refs. 20 and 26 for the exact results of the model at 1/4 and 1/2 fillings, respectively. Here, we will use both the bonding/antibonding basis set, which is conceptually similar to a molecular-like basis set, and the site basis, which can be considered as an atomic-like basis set (see Appendix A). The bonding/antibonding basis diagonalizes the one-body density matrix of the fully symmetric dimer, i.e., this basis set is the basis of natural orbitals. The site basis, instead, is the basis of natural orbitals for the symmetry-broken dimer. The site basis

offers a clearer picture of electron addition and removal for the Hubbard model, where the electron-electron interaction is on site. The eigenstates of the Hubbard Hamiltonian are given as linear combinations of Slater determinants built from the bonding/antibonding or the site basis functions. In the following, the notation $|A\sigma, B\sigma', \ldots\rangle$ indicates a Slater determinant with on its diagonal an electron in the orbital A with spin σ, an electron in the orbital B with spin σ', and so on. In the case of one electron, the Slater determinant $|A\sigma\rangle$ is a one-electron function.

A. Total energy and occupation numbers

1. 1/4 filling

In the case of the Hubbard dimer at 1/4 filling, the ground-state wavefunction reads as $|\Psi_0\rangle = |b\uparrow\rangle$ in the bonding/antibonding basis, i.e., one single Slater determinant with one spin-up electron in the bonding orbital (equivalently, the spin-down situation could be chosen). The exact one-body density matrix is idempotent for any U/t value at zero temperature, with the occupation number of the bonding (antibonding) orbital $n_{b\uparrow} = 1$ and $n_{b\downarrow} = 0$ ($n_{a\uparrow} = n_{a\downarrow} = 0$) (see Fig. 1,[77] upper panel). When projected on the site basis, one gets $|\Psi_0\rangle = (|1\uparrow\rangle + |2\uparrow\rangle)/\sqrt{2}$. This means that the electron has equal probability 1/2 of being on site 1 or site 2. Often, the electronic structure is probed by electron addition or removal, like in inverse or direct photoemission experiments. In the atomic limit (small hopping $t \to 0$, for which $U/t \to \infty$ for U fixed), one can imagine that the electron spends a long time on one site; there are therefore two possible addition energies: one at ϵ_0 when the addition electron goes to the unoccupied site and one at $\epsilon_0 + U$ when it goes to the occupied one. In this case, there is no correlation in the ground state, since the occupation numbers are zero or one, but electron addition leads to two strongly correlated electrons: the added electron has to see the electron in the system. When we use the Müller functional ($\alpha = 0.5$ in Eq. (4)), the optimal occupation numbers $n_{b\uparrow}$ and $n_{a\uparrow}$ tend to 0.5 with increasing U/t (see Fig. 1, upper panel). By increasing α up to 1 (Hartree-Fock), one approaches the exact situation; this is because exchange and Hartree energies completely cancel each other in the case of one electron. For comparison, we report also the results obtained using the functional proposed by Goedecker and Umrigar (GU)[57] and the so-called corrected Hartree-Fock (CHF) functional proposed by Csányi and Arias,[70] which are variants of the original Müller functional. The GU functional slows down the eventual merging of bonding and antibonding occupation numbers at 1/2, whereas the CHF is on top of the HF results for small interaction and tends towards the Müller results when increasing the interaction. Interestingly, the occupation numbers calculated from G_0W_0 are almost on top of the GU functional results. To obtain G_0W_0 occupation numbers, we use Eq. (11), with the G_0W_0 one-body Green's function on the right-hand side.

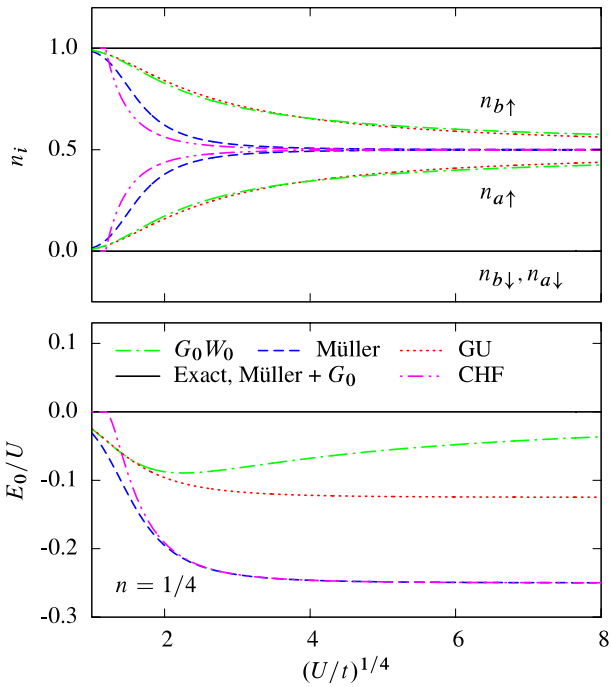

FIG. 1. Occupation numbers (upper panel) and total energy (lower panel) as function of U/t at 1/4 filling: exact vs. Müller functional, GU functional, CHF functional, and G_0W_0. Total energies obtained using G_0 occupation numbers in the Müller functional, and using the G_0W_0 Green's function in the Galitskii-Migdal formula (labelled Müller + G_0 and G_0W_0, respectively), are also reported.

Total energy results are reported in the lower panel of Fig. 1. All the approximations used underestimate the total energy, the exception being the Müller functional when fed with exact occupation numbers (obtained from G_0 at 1/4 filling[78]), which is on top of the exact result ("Müller + G_0" in Fig. 1). This finding is also observed at 1/2 filling. However, at one fourth filling, the exact occupation numbers being 1 or 0, any $0 \le \alpha \le 1$, would give the exact total energy. For comparison, we also reported the total energy obtained using Galitskii-Migdal equation (2) with the G_0W_0 Green's function, which is similar to the results obtained using the GU functional below $(U/t)^{1/4} \simeq 2$. In the atomic limit, however, the G_0W_0 total energy tends to the exact one as was already noticed in Ref. 20, whereas the GU functional gives a lower energy. For the CHF functional, we observe the same trend as for the occupation numbers.

In conclusion, at one fourth filling, we find that the Hartree-Fock approximation ($\alpha = 1$ in (4)) gives the exact occupation numbers, whereas the Müller functional ($\alpha = 0.5$ in (4)) gives results which quickly depart from the exact ones. Using the GU functional gives results in between these two extremes for any U/t; G_0W_0 occupation numbers are almost on top of the GU functional results. Finally, the CHF results are on top of the HF results at weak interaction, whereas they tend towards the Müller results for strong interaction. Concerning the total energy, all Müller-like functionals fed with exact occupation numbers give the exact results. All the other approximations tend to underestimate the total energy.

2. 1/2 filling

The wavefunction at 1/2 filling reads as $|\Psi_0\rangle = \sqrt{n_b}\,|b\uparrow, b\downarrow\rangle - \sqrt{n_a}\,|a\uparrow, a\downarrow\rangle$ (with $n_b = n_{b\uparrow} = n_{b\downarrow}$ and $n_a = n_{a\uparrow} = n_{a\downarrow}$) in the bonding/antibonding basis. Note that $|\Psi_0\rangle$ depends on the square root of the occupation numbers; the success of the Müller functional with $\alpha = 0.5$ at 1/2 filling

is linked to this. This functional is indeed closely related to the exact density-matrix functional for two-electron systems, which is the Löwdin-Shull functional.[71] The exact two-particle density matrix for such systems has an expansion in coefficients which are the square roots of the natural occupation numbers up to a sign.[72] A proper selection of the signs (which, in general, is unknown) gives the exact result for two-electron systems, which, for the Hubbard dimer, reads as $\Gamma^{(2)} = U/2 - U\sqrt{n_b n_a}$. At $U/t = 0$, the wavefunction is the single Slater determinant $|\Psi_0\rangle = |b\uparrow, b\downarrow\rangle$; increasing U/t, also the antibonding orbital becomes important, and eventually, the full wavefunction becomes a linear combination of the Slater determinants $|b\uparrow, b\downarrow\rangle$ and $|a\uparrow, a\downarrow\rangle$ with equal weight (see Fig. 2, upper panel). When projected on the site basis, the ground-state wavefunction reads as $|\Psi_0\rangle = A\,(|1\uparrow, 2\downarrow\rangle - |1\downarrow, 2\uparrow\rangle) + B\,(|1\uparrow, 1\downarrow\rangle - |1\downarrow, 1\uparrow\rangle)$, with $A = (\sqrt{n_b} + \sqrt{n_a})/2$ and $B = (\sqrt{n_b} - \sqrt{n_a})/2$ (see Ref. 20 and Appendix A). This means that for the noninteracting case ($n_b = 1$ and $n_a = 0$), each of the two electrons is equally distributed between the two sites, while increasing the interaction (n_b, $n_a \to 1/2$), double occupancies become less probable.

From Fig. 2, we see that the optimal occupation numbers for the Müller functional are the exact ones. The occupation numbers obtained using the CHF functional become quickly exact by increasing the interaction. Using the GU functional as well as varying α in the range 0.5-1 spoils this result. Again, G_0W_0 occupation numbers are very similar to the GU results. Note that G_0W_0 produces fractional occupation numbers with increasing U/t; eventually, they go to 1/2 at $t = 0$, but they go too slowly. This means that at strong interaction, G_0W_0 does not manage to well localize the two electrons, each on one site, and spurious double occupancies are still present.

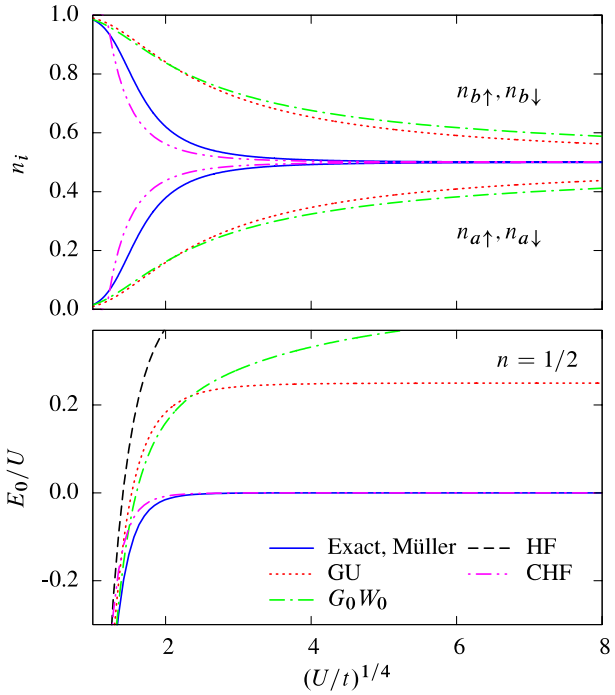

FIG. 2. Occupation numbers (upper panel) and total energy (lower panel) as function of U/t at 1/2 filling: exact vs. Müller functional, GU functional, CHF functional, and G_0W_0. The G_0W_0 total energies are obtained using the Galitskii-Migdal formula.

Total energies are reported in the lower panel of Fig. 2. The total energy within the Müller approximation is exact. The CHF total energy is on top of the HF total energy at weak interaction and merges with the exact result when increasing the interaction. The G_0W_0 result is similar to the result obtained using the GU functional below $(U/t)^{1/4} \simeq 3$; for stronger interaction, they differ, but both overestimate the total energy. Our G_0W_0 result is in line with previous GW calculations on the H_2 molecule,[22,50] which show GW to be very accurate close to equilibrium but to dramatically overestimate the total energy in the dissociation limit.[79] Comparison with recent total energy calculations on the Hubbard dimer[51] using the correlation energy expression obtained with the adiabatic-connection technique (see, e.g., Ref. 49) shows that RPA and beyond RPA including excitonic effects give better results than G_0W_0 at strong interaction.[80]

In conclusion, at one half filling, the Müller functional gives the exact occupation numbers. The CHF functional gives results similar to HF at weak interaction but rapidly similar to the exact results by increasing the interaction. G_0W_0 and the GU functional give similar occupation numbers, which merge with the exact ones at $t = 0$, but at a lower speed than the exact values. This reflects the fact that these two approximations have difficulties to localize the two electrons, one on each site, missing the atomic physics of strongly correlated electrons. Concerning the total energy, both G_0W_0 and GU similarly overestimate the exact values, whereas the Müller functional gives the exact result. The CHF functional becomes rapidly exact with the interaction. Increasing α leads to higher total energies, with HF giving the worst agreement ($E_0/U = -2t/U + 1/2$).

B. Removal/addition energies and spectral function

Exact removal and addition energies are reported in Figs. 3, 4, 5, and 6. We analyze various ways to compute removal/addition energies within RDMFT, which elucidate the role played by an approximate exchange-correlation energy functional and by an approximate expression for the removal/addition energies. First, we test the Müller-like approximations to the xc functional by combining the latter with the method proposed by Pernal and Cioslowski (EKT)[36] for the calculation of removal energies. This method, based on the extended Koopmans theorem, gives the exact removal energies of the Hubbard dimer at 1/4 and 1/2 fillings, when combined with the exact exchange-correlation energy functional. This allows us to study the accuracy of the xc functional approximations. Second, we test the DIF/DER method for the calculation of removal/addition energies by combining it with the exact xc functional. We then test the combination of the DIF/DER method and the Müller-like approximations to the xc energy functional.

Finally, we combine the DIF/DER method and the Müller-like functionals with the approximate expression for the spectral function given in Eq. (7). This is the approach used for the calculation of spectral functions of transition metal oxides already mentioned before.[33]

Exact, G_0W_0, and DIF/DER (within the Müller functional) spectral functions are compared in Figs. 7 and 8.

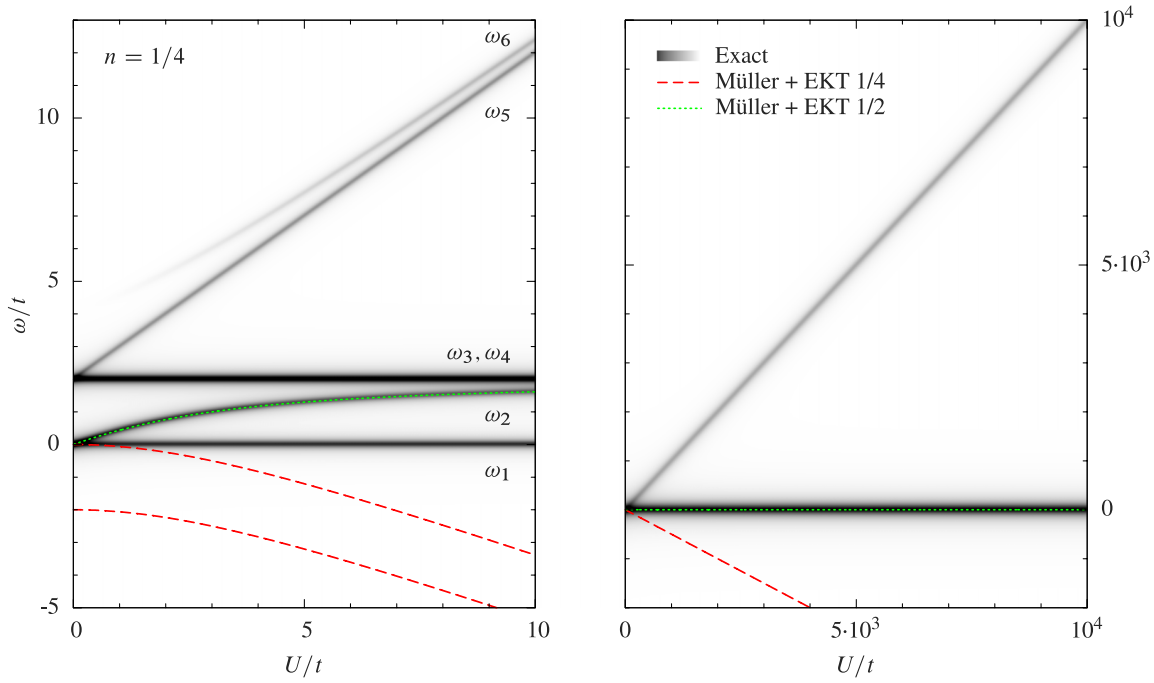

FIG. 3. Removal and addition energies ω/t as function of U/t at 1/4 filling: exact *vs*. EKT method used with the Müller functional (the label "Müller + EKT 1/4" refers to the removal energies, whereas "Müller + EKT 1/2" to the lowest addition energy calculated from the highest removal energy of the system at 1/2 filling). The labels ω_i indicate the exact energies. The color gradient (from white to black) of the exact curves indicates increasing spectral weight; the energy ω_6 is hence a satellite, since it has vanishing spectral weight at vanishing interaction. The addition energy "Müller + EKT 1/2" is on top of the exact energy ω_2, which goes to a constant at strong interaction (right panel).

1. 1/4 filling

At 1/4 filling, the Hubbard dimer shows five quasiparticle energies (one removal, labelled ω_1 in Fig. 3, and four addition energies (ω_2, ω_3, ω_4, ω_5)) and one addition satellite energy (ω_6). Satellites are weak removal or addition energies which acquire spectral weight with increasing interaction, whereas the intensity of quasiparticles decreases or remains constant. If the exact energy functional is used (which, for one-electron, is just $E = E_{\text{kin}} + E_{\text{ext}}$), then the EKT method produces the

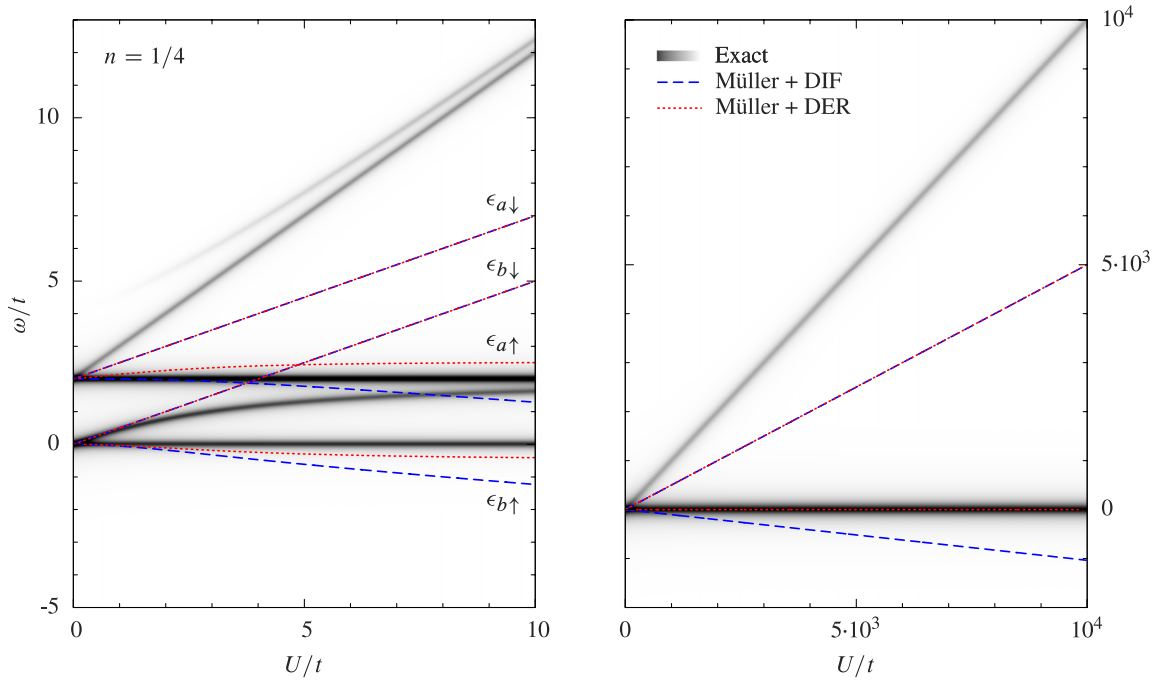

FIG. 4. Removal and addition energies ω/t as function of U/t at 1/4 filling: exact *vs*. DIF and DER methods used with the Müller functional. The labels ϵ_i indicate the bonding/antibonding energies obtained using the DIF/DER methods. The color gradient of the exact curves has the same meaning as in Fig. 3. The energies $\epsilon_{b\downarrow}$ and $\epsilon_{a\downarrow}$ calculated with the DIF method are on top of those obtained with the DER method and go as $U/(2t)$ at strong interaction (right panel); the energies $\epsilon_{b\uparrow}$ and $\epsilon_{a\uparrow}$ calculated with the DER method reach a constant value at strong interaction (right panel).

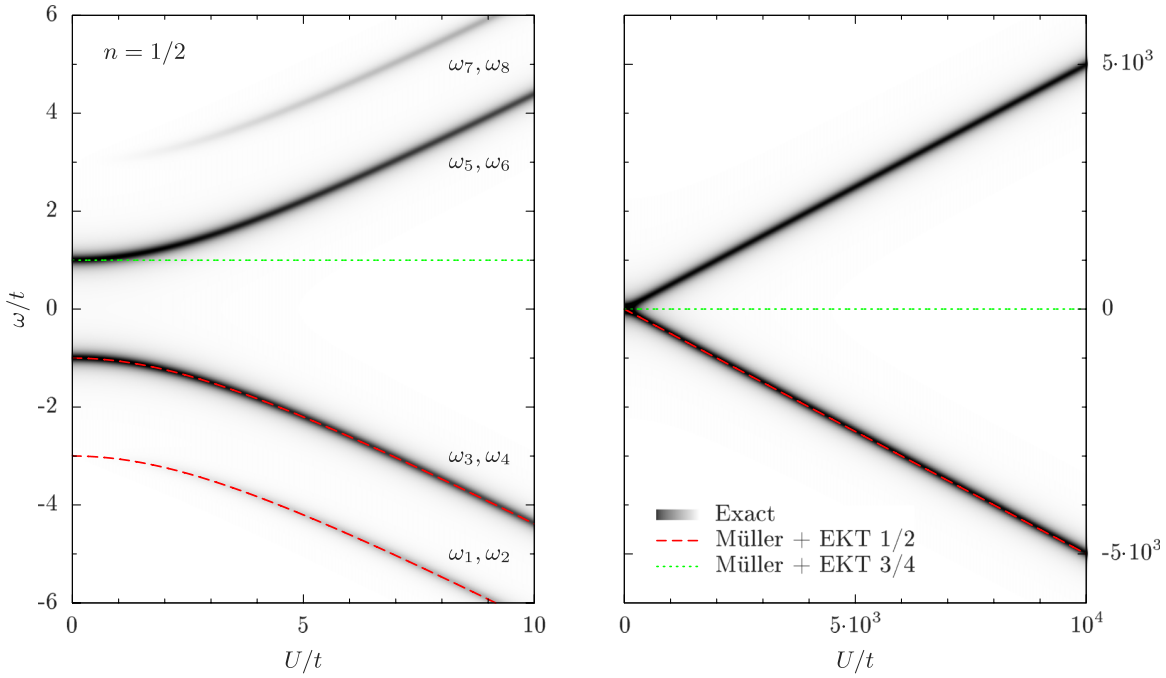

FIG. 5. Removal and addition energies ω/t as function of U/t at 1/2 filling: exact *vs*. EKT method used with the Müller functional (the label "Müller + EKT 1/2" refers to the removal energies, whereas "Müller + EKT 3/4" to the lowest addition energy calculated from the highest removal energy of the system at 3/4 filling). The labels ω_i indicate the exact energies. The color gradient (from white to black) of the exact curves indicates increasing spectral weight; the energies ω_1, ω_2, ω_7, ω_8 are hence satellites, since they have vanishing spectral weight at vanishing interaction.

exact removal energy $\epsilon_0 - t$ (ω_1 in Fig. 3). Using the Müller functional, instead, the EKT produces two removal energies (see result "Müller + EKT 1/4" in Fig. 3). This is due to the fact that within this functional, the antibonding occupation number $n_{a\uparrow}$ is not zero,[81] and therefore more degrees of freedom are added to the problem. The energies do not match well with the exact results. In the limit $U/t \to \infty$, the two removal energies merge together at a value well off the exact one (see right panel of Fig. 3). In this limit, the exact energies merge towards ϵ_0 and $\epsilon_0 + U$: this reflects the fact that in this limit, the electron has equal probability to localize on one site or the other of the dimer; therefore, one can have removal and addition energies (for a spin-down or a spin-up electron added to the empty site) at ϵ_0 and an addition energy at $\epsilon_0 + U$ (for a spin-down electron added to the site with one spin-up electron already present). We note that improvements are obtained changing α from 0.5 to 1

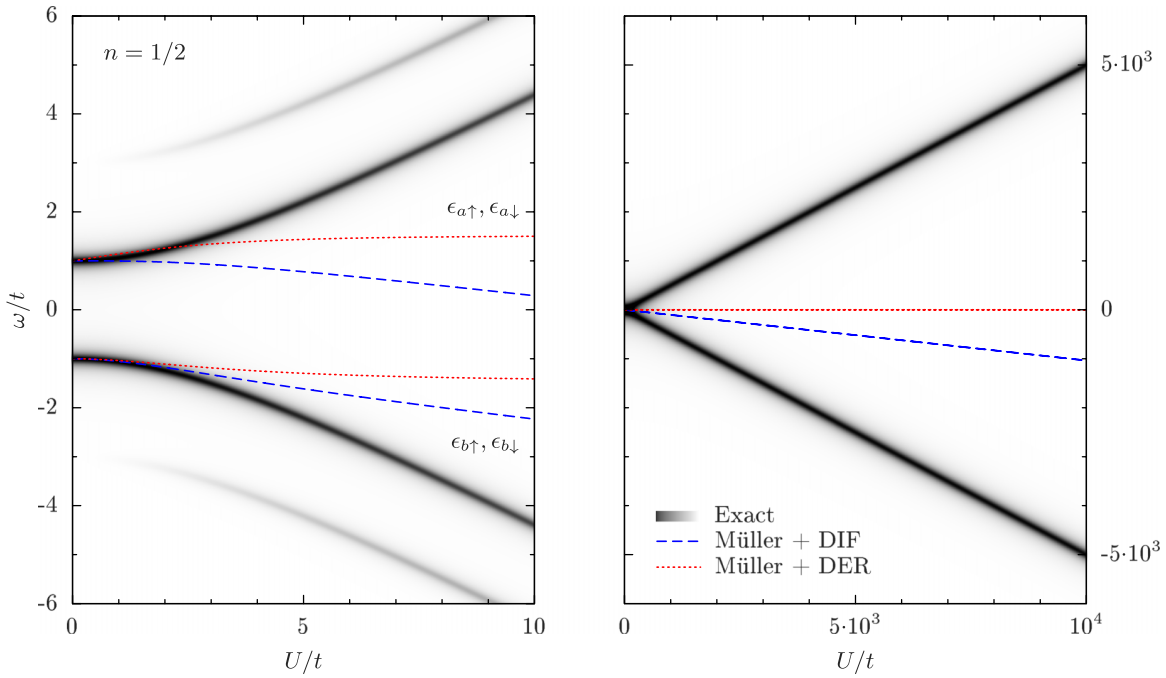

FIG. 6. Removal and addition energies ω/t as function of U/t at 1/2 filling: exact *vs*. DIF and DER methods used with the Müller functional. The labels ϵ_i indicate the bonding/antibonding energies obtained using the DIF/DER methods. The color gradient of the exact curves has the same meaning as in Fig. 5.

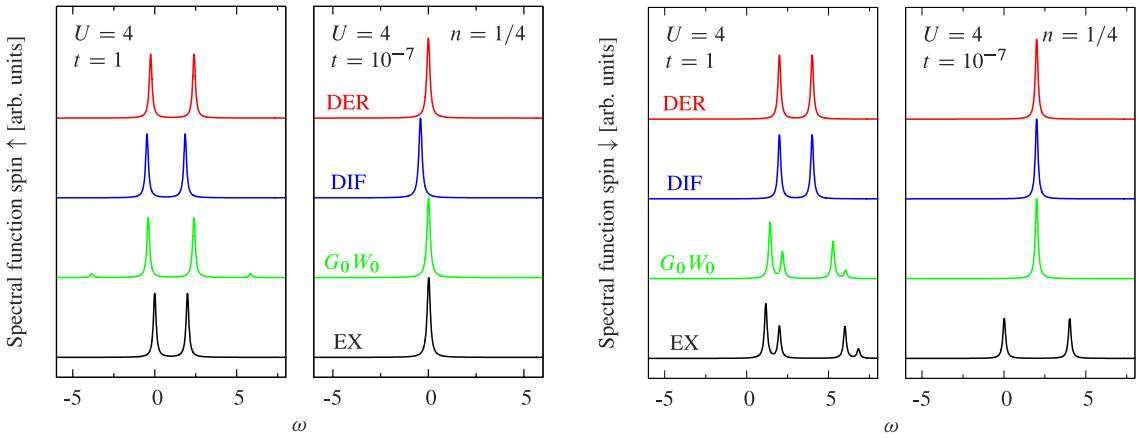

FIG. 7. Spectral function at 1/4 filling: exact *vs.* G_0W_0, and DER and DIF methods using the Müller functional.

(Hartree-Fock) as the exact functional is approached. Hartree-Fock, indeed, gives the exact total energy at 1/4 filling, due to an exact cancellation between Hartree and exchange energies. If the lowest addition energy is calculated from the highest removal energy of the system at 1/2 filling, the EKT yields the exact result (see result "Müller + EKT 1/2" in Fig. 3) but only because the Müller functional gives the exact total energy and occupation numbers at 1/2 filling (N + 1-electron system).

The DIF/DER method (Eqs. (8) and (12)) performs as the EKT if the exact xc functional is used: it produces the exact removal energy and the exact second lowest addition energy. With the Müller functional, it gives four energies (see result "Müller + DIF/DER" in Fig. 4): only two energies are in good agreement with the exact ones ($\epsilon_{b\uparrow}$ and $\epsilon_{a\uparrow}$, calculated from $n_{b\uparrow}$ and $n_{a\uparrow}$, respectively), whereas for the other two ($\epsilon_{b\downarrow}$ and $\epsilon_{a\downarrow}$), we observe that each is approximately an average of two exact ones, namely, $\epsilon_{b\downarrow}$ is an average of ω_2 and ω_6[82] and $\epsilon_{a\downarrow}$ of ω_3 (or, equivalently, ω_4) and ω_5. This can be understood considering that the $G_{b\uparrow}$ and $G_{a\uparrow}$ components of the one-body Green's functions have only one pole, whereas $G_{b\downarrow}$ and $G_{a\downarrow}$ have two poles each; the corresponding occupation numbers (see Eq. (11)) hence reflect these features.

In general, the spectral function profile is in overall good agreement with the exact one at moderately strong interaction U/t. For the spin-down channel (right panel of Fig. 7), G_0W_0 is slightly superior. It shows a very weak spurious satellite due to self-screening[20] in the spin-up channel, but it correctly describes the spin-down satellite. In the atomic limit ($t \to 0$), both DIF and DER methods show the same failure as G_0W_0: for the spin-down spectral function, the poles merge at $\epsilon_0 + U/2$, unlike the exact result which shows a gap equal to U. We observe the same scenario increasing the number of sites (not shown). The GU functional does not add any significant improvement to the picture, whereas the CHF functional gives the HF result for any t. If the lowest addition energy (spin-down channel) is calculated from the highest removal energy of the N + 1-electron system (1/2 filling), the method produces a gap, unlike the exact result, where the lowest addition energy coincides with the highest removal energy (ϵ_0). A similar error is found also in GW and it is a consequence of the self-screening error GW suffers from.[20]

In conclusion, combining the approximate Müller-like functionals with the DIF/DER method significantly improves electron addition and removal energies seen as poles in the spectral function with respect to the case where this functional is used with the more advanced EKT. This indicates that there is a cancellation of errors between the approximate Müller functional and the DIF/DER method, at least at 1/4 filling.

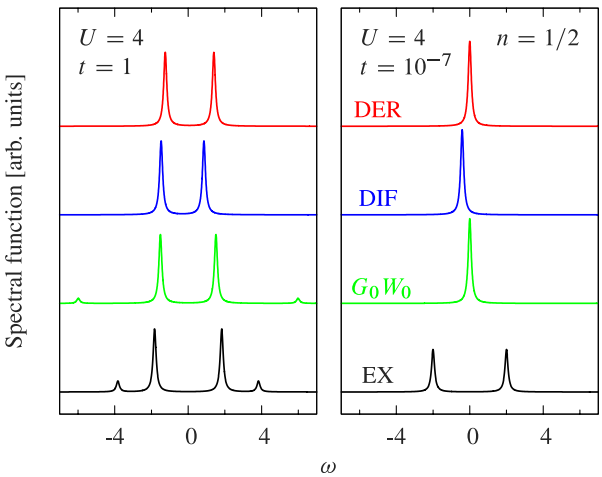

FIG. 8. Spectral function at 1/2 filling: exact *vs.* G_0W_0, and DER and DIF methods using the Müller functional.

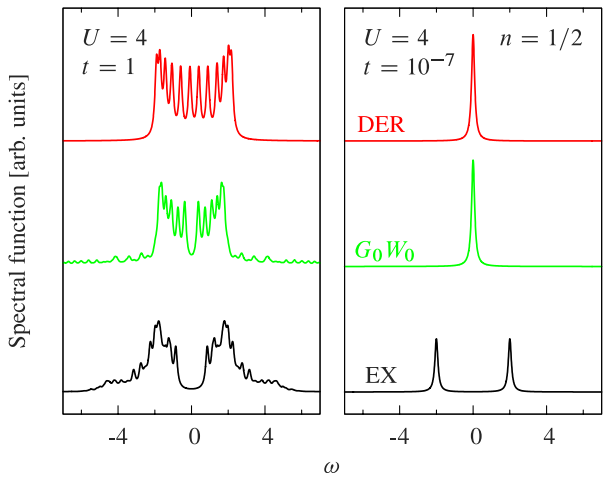

FIG. 9. Spectral function for a chain of 12 sites at 1/2 filling: exact *vs.* G_0W_0 and DER method using the Müller functional.

2. 1/2 filling

At 1/2 filling, there are four quasiparticle energies (labeled ω_3, ω_4, ω_5, ω_6, in Fig. 5) and four satellites (ω_1, ω_2, ω_7, ω_8). Using the Müller functional, which, in this case, gives the exact total energy and occupation numbers, the EKT gives two doubly degenerate energies: these are the exact removal energies, including a satellite. To get the lowest addition energy, one has to look at the $N+1$-electron system (3/4 filling); in this case, the Müller functional does not reproduce the exact total energy and occupation numbers and, consequently, the EKT gives an addition energy that strongly departs from the exact one as U/t increases.

Both DIF and DER methods give only two energies per spin channel, but their nature is in fact a mixture of quasiparticle and satellite energies and of electron addition and removal; for example, we found that the energy $\epsilon_{b\uparrow}$ in Fig. 5 is roughly a weighted average of the satellite and quasiparticle energies ω_3 and ω_7, respectively. Again, this can be understood by considering that the components $G_{b\sigma}$ and $G_{a\sigma}$ have two poles each, and therefore the corresponding occupation numbers reflect these features in the excitation energies $\epsilon_{b\sigma}$ and $\epsilon_{a\sigma}$. The results are quite different from the EKT, where one has both the removal quasiparticle and satellite energies. Since at 1/2 filling, the Müller functional is exact, there is not the same cancellation of error as observed at 1/4 filling, and the DER/DIF method introduces, hence, quite a large error.

In Fig. 8, we report the exact spectral function in comparison to the spectral functions obtained with G_0W_0 and DIF/DER using the Müller functional. Only two peaks appear in the DIF/DER spectra, which merge in the $t \to 0$ limit both for the DIF and DER methods. We note that the GU functional tends to open the gap, but it is not enough in the strongly correlated dissociation limit, whereas the CHF functional gives the HF results for any t. Changing α does not improve the situation. DIF and DER, therefore, perform as bad as G_0W_0 in the atomic limit, whereas G_0W_0 is significantly superior at moderately strong interaction. We note that this conclusion is not restricted to the Hubbard dimer; we find the same scenario by increasing the number of sites, as illustrated in Fig. 9 for a chain of 12 sites at 1/2 filling. However, if the lowest addition energy is calculated from the highest removal energy of the $N+1$-electron system, the DIF/DER method yields a gap at best half of the exact one in the atomic limit.

In conclusion, using an exact xc functional, the method of Ref. 33 has a large deviation from the exact results, both in the values and nature of the removal and addition energies. For moderately strong interaction, G_0W_0 is clearly superior. In the atomic limit, no gap is observed, as in GW, unless the $N+1$-electron system is considered for the calculation of the lowest addition energy.

IV. OCCUPATION NUMBERS AND CORRELATION

Occupation numbers are an indicator of correlation. However, what is observed is a result of measurements, and measurements change the system. One hence cannot look only at the occupation numbers of the initial system to understand observed correlation effects. For example, in Sec. III A 1, the Hubbard dimer at 1/4 filling has exact occupation numbers that are either zero or one. This is a clear example in which the occupation numbers indicate no correlation in the system, but there are correlation effects in the electron addition spectrum that one would measured, e.g., in inverse photoemission. In this case, indeed, the spectrum shows, besides quasiparticle peaks, also a satellite (ω_6 in Fig. 3), which is a pure signature of correlation. Therefore, whether a system "is" correlated or not depends on how one looks at it.

Let us examine this point further, by looking at the Hubbard dimer at 1/2 filling as example. In the atomic limit, the spin-singlet ground state $|\Psi_0\rangle = 1/\sqrt{2}[|1\uparrow,2\downarrow\rangle - |1\downarrow,2\uparrow\rangle]$ becomes degenerate with the spin-symmetry broken state $|\Psi_0\rangle = |1\uparrow,2\downarrow\rangle$ (or, equivalently, $|\Psi_0\rangle = |1\downarrow,2\uparrow\rangle$), which is also an eigenstate of the system in this limit. We note that in the spin-symmetry broken case, both G_0W_0 and RDMFT within the Müller functional give the exact result for total energy, occupation numbers, and spectral function[83] (see Appendix B for more details). In this case, the electrons have fixed positions and one does not need to consider explicitly the correlation between two particles. One can hence think that there is little correlation in this state. In reality, the system is correlated, but part of the correlation is included in the symmetry breaking.

A. Spectral function

Let us first focus on the spectral function. From Fig. 8, we see that the exact spectral function of the spin singlet (lowest right panel) shows two peaks, one at ϵ_0 and one at $\epsilon_0 + U$, both for spin-up and spin-down channels. For the spin-symmetry broken case, the components of the one-body Green's functions show the spin-symmetry breaking nature of the ground state, i.e., $G_{ii\uparrow} \neq G_{ii\downarrow}$ and $G_{11\uparrow} = G_{22\downarrow}$, $G_{11\downarrow} = G_{22\uparrow}$ and hence are different from the ones of the singlet case (all diagonal components are the same and all off-diagonal components are the same). However, the spin-resolved total spectral function, i.e., $A_\sigma(\omega) = \sum_i |\Im G_{ii\sigma}(\omega)|/\pi$, is the same for the two spin structures: one can remove a spin-up or spin-down electron with energy ϵ_0 and can add a spin-up or spin-down electron with energy $\epsilon_0 + U$.[84]

B. Momentum distribution

Can the occupation numbers distinguish between the spin-singlet and spin-symmetry broken states? For the spin-singlet structure, the natural orbitals are the bonding/antibonding orbitals and the occupation numbers are $n_{b\uparrow} = n_{b\downarrow} = 1/2$ and $n_{a\uparrow} = n_{a\downarrow} = 1/2$ (see Fig. 2). For the spin-symmetry broken structure, characterized by a single Slater determinant, the natural orbitals are the site orbitals $\psi_{1\sigma/2\sigma} = (\phi_{b\sigma} \pm \phi_{a\sigma})/\sqrt{2}$ with occupation numbers $n_{1\uparrow} = n_{2\downarrow} = 1$ and $n_{1\downarrow} = n_{2\uparrow} = 0$. Spin-resolved occupation numbers are, hence, different for the two spin structures. It is now interesting to examine whether this difference could be measured.

The most direct experimental route to access occupation numbers is Compton scattering. The Compton profile gives information about the momentum distribution, i.e., the probability to observe a particle of momentum $\mathbf{p}$ (see, e.g., Refs. 73 and 74). This can be expressed in terms of the Fourier transform in momentum space of the density matrix, as

$$n(\mathbf{p}) \propto \int d\mathbf{r}d\mathbf{r}' e^{-i\mathbf{p}\cdot(\mathbf{r}-\mathbf{r}')}\gamma(\mathbf{r},\mathbf{r}'), \tag{15}$$

where we defined $\gamma(\mathbf{r},\mathbf{r}') = \sum_\sigma \sum_{ss'} \chi^*_\sigma(s)\gamma(\mathbf{x},\mathbf{x}')\chi_\sigma(s')$, with $\chi_\sigma(s)$ the spin function, which is defined as $\chi_\uparrow(1/2) = \chi_\downarrow(-1/2) = 1$ and $\chi_\uparrow(-1/2) = \chi_\downarrow(1/2) = 0$. Fourier transform (15) gives the matrix elements of the density matrix in a basis of plane waves $\phi_{p\sigma}(\mathbf{r},s) = 1/\sqrt{\Omega}\, e^{i\mathbf{p}\cdot\mathbf{r}}\chi_\sigma(s)$, which are the exact one-electron eigenfunctions of the free electron gas, i.e., the perfectly translationally invariant system. The question is hence what one could observe looking at matrix elements of the density matrix in the basis of plane waves. The analogous basis for the Hubbard dimer which reflects the symmetry of the system is the bonding/antibonding basis $\{\phi_{b\sigma/a\sigma}\}$. Since this basis is the basis of natural orbitals for the spin-singlet system, in this case the analog of the Compton profile gives the occupation numbers $n_b = 1$ (with $n_{b\uparrow} = n_{b\downarrow} = 1/2$) and $n_a = 1$ (with $n_{a\uparrow} = n_{a\downarrow} = 1/2$). One gets the same result for the spin-symmetry broken structure. Note, however, that in this case, unlike for the spin-singlet structure, this distribution corresponds to density-matrix elements that are not occupation numbers. This is because the bonding/antibondig basis in which the density matrix is projected is not the basis of natural orbitals for the spin-symmetry broken structure. In fact, not even a spin-resolved "Compton profile" would distinguish between the two spin structures, since for the spin-broken symmetry structure, one gets the density-matrix elements $n_{b\sigma/a\sigma} = \int d\mathbf{x}d\mathbf{x}' \phi^*_{b\sigma/a\sigma}(\mathbf{x}) \left[\sum_{i=1\uparrow,2\downarrow} \psi_i(\mathbf{x})\psi^*_i(\mathbf{x}')\right] \phi_{b\sigma/a\sigma}(\mathbf{x}') = 1/2$, as for the spin-singlet case. To distinguish between the two cases, one should measure other aspects of the density matrix, for example, carry out a spin- and space-resolved measurement of the density matrix elements. In this case, the density matrix is projected in the site basis, which gives the density matrix elements $n_{1\uparrow} = n_{2\uparrow} = n_{1\downarrow} = n_{2\downarrow} = 1/2$ for the spin-singlet and the occupation numbers $n_{1\uparrow} = n_{2\downarrow} = 1$, $n_{1\downarrow} = n_{2\uparrow} = 0$ for the spin-symmetry broken case.

V. CONCLUSIONS

We analyzed the results for total energy, natural occupation numbers, removal/addition energies, and spectral function for the Hubbard dimer at 1/4 and 1/2 fillings by using reduced density-matrix functional theory and many-body perturbation theory within standard approximations to electron correlation, namely, Müller-like functionals and G_0W_0, respectively. In general, there is no Müller-like functional which works well at both one fourth and half filling: for the former, the Hartree-Fock functional gives the exact total energy and occupation numbers, whereas for the latter, the original Müller functional does the job. Other Müller-like functionals underestimate the total energy at 1/4 filling and overestimate it at 1/2 filling, like G_0W_0. The same behavior is found for the occupation numbers, which deviate in a similar way as G_0W_0 from the exact results.

We also analyzed various approximate methods to obtain removal/addition energies and spectral functions from RDMFT. Our results using the extended Koopmans theorem confirm its reliability for the calculation of removal energies and the lowest addition energy (for finite systems), if a good approximation to the two-body density matrix is used. However, the calculation of the addition energy relies on the N+1-electron system; in this case, one has an anion, which might not be stable. Moreover, the EKT does not give higher addition energies nor the spectral function. These can be obtained using the approximate DIF/DER method. However, our results suggest a cancellation of errors between this method and Müller-like approximations to electron correlations. Moreover, we find that the spectral peaks are fewer than the exact ones and can have a mixed removal and addition nature as well as a mixed quasiparticle and satellite nature. These findings indicate that although an *ab initio* simulation of the spectral function of a real material using the DIF/DER method could be in agreement with experiment, the underlying physics is not correct. Our analysis shows that the failure of the DIF/DER method is mainly due to the approximation of removal/addition energies, rather than to the approximation of the spectral function itself. Therefore, one should focus on better approximations to these energies, to improve the description of photoemission spectra. Work in this direction is currently in progress.

At moderately strong interaction, the G_0W_0 method is superior. In the strongly correlated electron regime, which is obtained by stretching the dimer (atomic limit), we found that both the DIF/DER method and G_0W_0 fail for a spin-singlet ground state, whereas they give the exact results for the spin-symmetry-broken case.

Because the Hubbard dimer is a simple test case, it shines light on the content, successes, and limits of current RDMFT approaches and we believe that arguments like those based on symmetry and symmetry breaking can be safely generalized to improve our understanding of real systems.

ACKNOWLEDGMENTS

The research leading to these results has received funding from the European Research Council under the European Union's Seventh Framework Programme (No. FP/2007—2013)/ERC Grant Agreement No. 320971. Discussion within the Collaboration Team on Correlation of the European Theoretical Spectroscopy Facility (ETSF) is greatly acknowledged. S.D.S. and P.R. thank S. Sharma, N. N. Lathiotakis, and F. G. Eich for fruitful discussions.

APPENDIX A: BONDING-ANTIBONDING BASIS

The bonding/antibonding basis $\{\phi_i\}$ is defined as

$$\phi_{b\sigma} = \frac{1}{\sqrt{2}}\psi_{1\sigma} + \frac{1}{\sqrt{2}}\psi_{2\sigma}, \tag{A1}$$

TABLE I. Coefficients of the transformation from site to bonding/antibonding basis for 1 electron.

	$\lvert b\uparrow\rangle$	$\lvert b\downarrow\rangle$	$\lvert a\uparrow\rangle$	$\lvert a\downarrow\rangle$
$\lvert 1\uparrow\rangle$	$1/\sqrt{2}$	0	$1/\sqrt{2}$	0
$\lvert 1\downarrow\rangle$	0	$1/\sqrt{2}$	0	$1/\sqrt{2}$
$\lvert 2\uparrow\rangle$	$1/\sqrt{2}$	0	$-1/\sqrt{2}$	0
$\lvert 2\downarrow\rangle$	0	$1/\sqrt{2}$	0	$-1/\sqrt{2}$

TABLE II. Coefficients of the transformation from site to bonding/antibonding basis for 2 electrons.

	$\|b\uparrow,b\downarrow\rangle$	$\|b\uparrow,a\uparrow\rangle$	$\|b\uparrow,a\downarrow\rangle$	$\|b\downarrow,a\uparrow\rangle$	$\|b\downarrow,a\downarrow\rangle$	$\|a\uparrow,a\downarrow\rangle$
$\|1\uparrow,2\downarrow\rangle$	1/2	0	−1/2	−1/2	0	−1/2
$\|1\downarrow,2\uparrow\rangle$	−1/2	0	−1/2	−1/2	0	1/2
$\|1\uparrow,2\uparrow\rangle$	0	−1	0	0	0	0
$\|1\downarrow,2\downarrow\rangle$	0	0	0	0	−1	0
$\|1\uparrow,1\downarrow\rangle$	1/2	0	1/2	−1/2	0	1/2
$\|2\uparrow,2\downarrow\rangle$	1/2	0	−1/2	1/2	0	1/2

TABLE III. Eigenvalues and expansion coefficients of the eigenstates in the bonding/antibonding basis for the two-electron system.

E_i	$\|b\uparrow,b\downarrow\rangle$	$\|b\uparrow,a\uparrow\rangle$	$\|b\uparrow,a\downarrow\rangle$	$\|b\downarrow,a\uparrow\rangle$	$\|b\downarrow,a\downarrow\rangle$	$\|a\uparrow,a\downarrow\rangle$
$2\epsilon_0+(U-c)/2$	$(1+4t/(c-U))/a$	0	0	0	0	$(1-4t/(c-U))/a$
$2\epsilon_0+(U+c)/2$	$(1-4t/(c+U))/b$	0	0	0	0	$(1+4t/(c+U))/b$
$2\epsilon_0+U$	0	0	$-1/\sqrt{2}$	$1/\sqrt{2}$	0	0
$2\epsilon_0$	0	0	0	0	−1	0
$2\epsilon_0$	0	−1	0	0	0	0
$2\epsilon_0$	0	0	$-1/\sqrt{2}$	$-1/\sqrt{2}$	0	0

$$\phi_{a\sigma}=\frac{1}{\sqrt{2}}\psi_{1\sigma}-\frac{1}{\sqrt{2}}\psi_{2\sigma}, \tag{A2}$$

where $\{\psi_i\}$ is the site basis.

In Ref. 20, the results of the Hubbard dimer 1/4 and 1/2 fillings are given using a basis of Slater determinants $|\ldots\rangle$ constructed using the site basis. In Tables I and II, we give the transformation of this Slater determinants from the site basis to the bonding/antibonding basis.

1. 1/4 filling

The eigenstates of the Hamiltonian at 1/4 filling are $|b\uparrow\rangle$ (the ground state), $|b\downarrow\rangle$, $|a\uparrow\rangle$, $|a\downarrow\rangle$ with energies ϵ_0-t, ϵ_0-t, ϵ_0+t, ϵ_0+t.

2. 1/2 filling

The eigenstates of the Hamiltonian at 1/2 filling in the bonding/antibonding representation are given in Table III. Here, $c^2=16t^2+U^2$, $a^2=2\left[16t^2/(c-U)^2+1\right]$, and $b^2=2\left[16t^2/(c+U)^2+1\right]$.

APPENDIX B: RDMFT FOR A SPIN-SYMMETRY BROKEN DIMER AT 1/2 FILLING

Any Müller-like functional gives the exact result for the total energy, the occupation numbers, and the spectral function calculated using the DIF method. Using the DER method, one gets the exact spectral function with $\alpha=1$ and 1/2. This is due to the extreme simplicity of the system in presence of symmetry breaking. In this case, indeed, the ground-state wavefunction reads as $|\Psi_0\rangle=|1\uparrow,2\downarrow\rangle$ (or, equivalently, $|\Psi_0\rangle=|1\downarrow,2\uparrow\rangle$), the natural orbitals are the site orbitals, and the occupation numbers are $n_{1\uparrow}=n_{2\downarrow}=1$ and $n_{1\downarrow}=n_{2\uparrow}=0$. The total energy, using a Müller-like functional, reads as

$$E[\{n_i\}]=\sum_{i,\sigma}h_i n_{i\sigma}+\frac{U}{2}\sum_{i,\sigma,\sigma'}n_{i\sigma}n_{i\sigma'}-\frac{U}{2}\sum_{i,\sigma}n_{i\sigma}^{2\alpha},$$

where $h_i=\epsilon_0$ and the sum runs over the sites. One can check that for the DIF method, one gets

$$\epsilon_{i\sigma}=h_i+Un_{i\bar{\sigma}}, \tag{B1}$$

where $\bar{\sigma}$ is the spin opposite of σ, for any $1/2\le\alpha\le1$, from which $\epsilon_{1\uparrow}=\epsilon_{2\downarrow}=\epsilon_0$ and $\epsilon_{1\downarrow}=\epsilon_{2\uparrow}=\epsilon_0+U$, as the exact result. For the DER method, one gets

$$\epsilon_{i\sigma}=h_i+\left(U\sum_{\sigma'}n_{i\sigma'}-\alpha Un_{i\sigma}^{2\alpha-1}\right)\Bigg|_{n_{i\sigma}=1/2}. \tag{B2}$$

For $\alpha=1$ and 1/2, the DER equation reduces to the DIF equation, which gives the exact spectral function. For other values of α, one gets $\epsilon_{1\uparrow}=\epsilon_{2\downarrow}=\epsilon_0+U/2-\alpha U/2^{2\alpha-1}$ and $\epsilon_{1\downarrow}=\epsilon_{2\uparrow}=\epsilon_{1\uparrow}+U$, which gives the exact band gap of U.

[1]M. Imada, A. Fujimori, and Y. Tokura, Rev. Mod. Phys. **70**, 1039 (1998).
[2]D. Ködderitzsch, W. Hergert, Z. Szotek, and W. M. Temmerman, Phys. Rev. B **68**, 125114 (2003).
[3]M. R. Norman, Science **332**, 196 (2003).
[4]M. Gatti, F. Bruneval, V. Olevano, and L. Reining, Phys. Rev. Lett. **99**, 266402 (2007).
[5]M. Springer, F. Aryasetiawan, and K. Karlsson, Phys. Rev. Lett. **80**, 2389 (1998).
[6]F. Aryasetiawan and O. Gunnarsson, Phys. Rev. Lett. **74**, 3221 (1995).
[7]S. Biermann, F. Aryasetiawan, and A. Georges, Phys. Rev. Lett. **90**, 086402 (2003).
[8]L. Hedin, Phys. Rev. **139**, A796 (1965).
[9]W. G. Aulbur, L. Jönsson, and J. W. Wilkins, Solid State Phys. **54**, 1 (1999), and references therein.
[10]F. Aryasetiawan and O. Gunnarsson, Rep. Prog. Phys. **61**, 237 (1998), and references therein.
[11]J. Vidal, S. Botti, P. Olsson, J. F. Guillemoles, and L. Reining, Phys. Rev. Lett. **104**, 056401 (2010).
[12]J. Vidal, X. Zhang, L. Yu, J.-W. Luo, and A. Zunger, Phys. Rev. B **84**, 041109 (2011).
[13]I. A. Nechaev, R. C. Hatch, M. Bianchi, D. Guan, C. Friedrich, I. Aguilera, J. L. Mi, B. B. Iversen, S. Blügel, P. Hofmann *et al.*, Phys. Rev. B **87**, 121111 (2013).

[14]D. Waroquiers, A. Lherbier, A. Miglio, M. Stankovski, S. Poncé, M. J. T. Oliveira, M. Giantomassi, G.-M. Rignanese, and X. Gonze, Phys. Rev. B **87**, 075121 (2013).
[15]E. Papalazarou, M. Gatti, M. Marsi, V. Brouet, F. Iori, L. Reining, E. Annese, I. Vobornik, F. Offi, A. Fondacaro *et al.*, Phys. Rev. B **80**, 155115 (2009).
[16]A. N. Chantis, M. van Schilfgaarde, and T. Kotani, Phys. Rev. B **76**, 165126 (2007).
[17]S. V. Faleev, M. van Schilfgaarde, and T. Kotani, Phys. Rev. Lett. **93**, 126406 (2004).
[18]L. Y. Lim, S. Lany, Y. J. Chang, E. Rotenberg, A. Zunger, and M. F. Toney, Phys. Rev. B **86**, 235113 (2012).
[19]W. Nelson, P. Bokes, P. Rinke, and R. W. Godby, Phys. Rev. A **75**, 032505 (2007).
[20]P. Romaniello, S. Guyot, and L. Reining, J. Chem. Phys. **131**, 154111 (2009).
[21]M. van Schilfgaarde, T. Kotani, and S. Faleev, Phys. Rev. Lett. **96**, 226402 (2006).
[22]A. Stan, N. E. Dahlen, and R. van Leeuwen, J. Chem. Phys. **130**, 114105 (2009).
[23]F. Caruso, P. Rinke, X. Ren, M. Scheffler, and A. Rubio, Phys. Rev. B **86**, 081102 (2012).
[24]M. Puig von Friesen, C. Verdozzi, and C.-O. Almbladh, Phys. Rev. Lett. **103**, 176404 (2009).
[25]V. P. Zhukov, E. V. Chulkov, and P. M. Echenique, Phys. Rev. Lett. **93**, 096401 (2004).
[26]P. Romaniello, F. Bechstedt, and L. Reining, Phys. Rev. B **85**, 155131 (2012).
[27]M. Guzzo, G. Lani, F. Sottile, P. Romaniello, M. Gatti, J. J. Kas, J. J. Rehr, M. G. Silly, F. Sirotti, and L. Reining, Phys. Rev. Lett. **107**, 166401 (2011).
[28]M. Guzzo, J. J. Kas, L. Sponza, C. Giorgetti, F. Sottile, D. Pierucci, M. G. Silly, F. Sirotti, J. J. Rehr, and L. Reining, Phys. Rev. B **89**, 085425 (2014).
[29]J. Lischner, D. Vigil-Fowler, and S. G. Louie, Phys. Rev. Lett. **110**, 146801 (2013).
[30]A. Grüneis, G. Kresse, Y. Hinuma, and F. Oba, Phys. Rev. Lett. **112**, 096401 (2014).
[31]G. Lani, P. Romaniello, and L. Reining, New J. Phys. **14**, 013056 (2012).
[32]J. A. Berger, P. Romaniello, F. Tandetzky, B. S. Mendoza, C. Brouder, and L. Reining, New J. Phys. **16**, 113025 (2014).
[33]S. Sharma, J. K. Dewhurst, S. Shallcross, and E. K. U. Gross, Phys. Rev. Lett. **110**, 116403 (2013).
[34]P.-O. Löwdin, Phys. Rev. **97**, 1474 (1955).
[35]T. L. Gilbert, Phys. Rev. B **12**, 2111 (1975).
[36]K. Pernal and J. Cioslowski, Chem. Phys. Lett. **412**, 71 (2005).
[37]O. W. Day, D. W. Smith, and C. Garrod, Int. J. Quantum Chem. **8**(S8), 501 (1974).
[38]M. M. Morrell, R. G. Parr, and M. Levy, J. Chem. Phys. **62**, 549 (1975).
[39]R. C. Morrison, J. Chem. Phys. **96**, 3718 (1992).
[40]D. Sundholm and J. Olsen, J. Chem. Phys. **98**, 3999 (1993).
[41]K. J. H. Giesbertz and R. van Leeuwen, J. Chem. Phys. **139**, 104109 (2013).
[42]K. J. H. Giesbertz and R. van Leeuwen, J. Chem. Phys. **139**, 104110 (2013).
[43]E. J. Baerends, Phys. Rev. Lett. **87**, 133004 (2001).
[44]M. Fuchs, Y.-M. Niquet, X. Gonze, and K. Burke, J. Chem. Phys. **122**, 094116 (2005).
[45]Q. Wu, C.-L. Cheng, and T. Van Voorhis, J. Chem. Phys. **127**, 164119 (2007).
[46]K. J. H. Giesbertz, E. J. Baerends, and O. V. Gritsenko, Phys. Rev. Lett. **101**, 033004 (2008).
[47]N. E. Dahlen, R. van Leeuwen, and U. von Barth, Phys. Rev. A **73**, 012511 (2006).
[48]A. Stan, N. E. Dahlen, and R. van Leeuwen, Europhys. Lett. **76**, 298 (2006).
[49]X. Ren, P. Rinke, C. Joas, and M. Scheffler, J. Mater. Sci. **47**, 7447 (2012).
[50]F. Caruso, D. R. Rohr, M. Hellgren, X. Ren, P. Rinke, A. Rubio, and M. Scheffler, Phys. Rev. Lett. **110**, 146403 (2013).
[51]T. Olsen and K. S. Thygesen, J. Chem. Phys. **140**, 164116 (2014).
[52]A. Fetter and J. D. Walecka, *Quantum Theory of Many-Particle Systems* (Dover Publications, 2003).
[53]L. Hedin, J. Phys.: Condens. Matter **11**, R489 (1999).
[54]O. Gritsenko, K. Pernal, and E. J. Baerends, J. Chem. Phys. **122**, 204102 (2005).
[55]M. A. Buijse, Ph.D. thesis, Vrije Universiteit Amsterdam, 1991.
[56]M. A. Buijse and E. J. Baerends, Mol. Phys. **100**, 401 (2002).
[57]S. Goedecker and C. J. Umrigar, Phys. Rev. Lett. **81**, 866 (1998).
[58]N. N. Lathiotakis, N. Helbig, and E. K. U. Gross, Phys. Rev. B **75**, 195120 (2007).
[59]M. Piris, Int. J. Quantum Chem. **113**, 620 (2013).
[60]S. Sharma, J. K. Dewhurst, N. N. Lathiotakis, and E. K. U. Gross, Phys. Rev. B **78**, 201103 (2008).
[61]A. Müller, Phys. Lett. A **105**, 446 (1984).
[62]N. N. Lathiotakis, S. Sharma, J. K. Dewhurst, F. G. Eich, M. A. L. Marques, and E. K. U. Gross, Phys. Rev. A **79**, 040501 (2009).
[63]A. Cohen and E. Baerends, Chem. Phys. Lett. **364**, 409 (2002).
[64]N. N. Lathiotakis and M. A. L. Marques, J. Chem. Phys. **128**, 184103 (2008).
[65]N. N. Lathiotakis, N. Helbig, A. Zacarias, and E. K. U. Gross, J. Chem. Phys. **130**, 064109 (2009).
[66]K. J. H. Giesbertz, Ph.D. thesis, Vrije Universiteit Amsterdam, 2010.
[67]E. N. Zarkadoula, S. Sharma, J. K. Dewhurst, E. K. U. Gross, and N. N. Lathiotakis, Phys. Rev. A **85**, 032504 (2012).
[68]D. A. Liberman, Phys. Rev. B **62**, 6851 (2000).
[69]J. Hubbard, Proc. R. Soc. A **276**, 238 (1963).
[70]G. Csányi and T. A. Arias, Phys. Rev. B **61**, 7348 (2000).
[71]P.-O. Löwdin and H. Shull, Phys. Rev. **101**, 1730 (1956).
[72]R. van Meer, O. V. Gritsenko, and E. J. Baerends, J. Chem. Phys. **140**, 024101 (2014).
[73]S. Huotari, J. A. Soininen, T. Pylkkänen, K. Hämäläinen, A. Issolah, A. Titov, J. McMinis, J. Kim, K. Esler, D. M. Ceperley *et al.*, Phys. Rev. Lett. **105**, 086403 (2010).
[74]V. Olevano, A. Titov, M. Ladisa, K. Hämäläinen, S. Huotari, and M. Holzmann, Phys. Rev. B **86**, 195123 (2012).
[75]Note that in practice, one often uses the Kohn–Sham G as starting point, instead of G_0.
[76]Note that in the functional originally considered by Müller, the exchange–correlation part of the two-body density matrix has the form $2\Gamma^{(2)}_{\rm xc}(\mathbf{x},\mathbf{x}';\mathbf{x},\mathbf{x}') = -\gamma^{1/2+p}(\mathbf{x},\mathbf{x}')\gamma^{1/2-p}(\mathbf{x}',\mathbf{x})$, with $-1/2 \le p \le 1/2$. With such a form, however, the probability of finding an electron at $\mathbf{r}$ when a second one is at $\mathbf{r}'$ becomes negative in the neighborhood of $\mathbf{r}'$. This error is minimized choosing $p = 0$.
[77]Note that here and in Fig. 2, we use $(U/t)^{1/4}$ on the horizontal axis to facilitate the comparison with Ref. 51 at 1/2 filling.
[78]For one electron, the hole part of the non-interacting Green's function, i.e., the part related to removal energies, is exact, because the removed electron does not interact with other electrons in the system; the exact occupation numbers can hence be calculated from G_0 according to Eq. (11).
[79]Note that at 1/2 filling, we use the particle–hole form of the Hubbard Hamiltonian.[26] In the G_0W_0 removal/addition energies, the particle–hole symmetry is lost for $U \neq 0$ due to the lack of self-consistency; we restore this symmetry by absorbing the static part of the self-energy $(U/2)$ into the chemical potential. This alignment of the chemical potential corrects for the lack of self-consistency.[8]
[80]Note that in Ref. 49, the authors chose $\epsilon_0 = 0$ and $V_0 = 0$ in the Hubbard Hamiltonian. A G_0W_0 calculation in this case gives a total energy better than the RPA total energy; in our calculations, instead, by restoring the particle–hole symmetry,[26] the GW spectral properties are improved, but the total energy worsens.
[81]Note that at $U = 0$, $n_{a\uparrow} = 0$ and the corresponding removal energy calculated with the EKT does not have a meaning. At $U = 0$, the EKT yields only the exact removal energy.
[82]Note that at $U = 0$, ω_6 has zero spectral weight.
[83]To be precise, RDMFT gives the exact total energy and occupation number for any Müller-like functional; the DIF method gives the exact spectral function for any Müller-like functional, whereas the DER method gives the exact results using Müller and HF.
[84]In real materials, this is often observed. For example, in NiO, no significant changes in the valence band structure are detected passing from the paramagnetic to the antiferromagnetc phase.